

# Data-Driven Feedforward Control for Suppressing Coupled Vibrations in Positioning Systems

1<sup>st</sup> Shota Teramoto  
*Dept. of Engineering*  
*Nagoya Institute of Technology*  
Nagoya, Japan  
s.teramoto.702@stn.nitech.ac.jp

3<sup>rd</sup> Shimpei Sato  
*Dept. of Engineering*  
*Nagoya Institute of Technology*  
Nagoya, Japan  
s.sato.770@nitech.jp

2<sup>nd</sup> Daigo Yamaguchi  
*Dept. of Engineering*  
*Nagoya Institute of Technology*  
Nagoya, Japan  
d.yamaguchi.619@stn.nitech.ac.jp

4<sup>th</sup> Yoshihiro Maeda  
*Dept. of Engineering*  
*Nagoya Institute of Technology*  
Nagoya, Japan  
ymaeda@nitech.ac.jp

**Abstract**—In the fast and precise control of positioning mechanisms, coupled vibrations often arise owing to the interaction of multiple structural components within industrial machines, leading to deteriorated positioning accuracy and increased complexity in controller design. This paper presents data-driven vibration suppression control (DD-VSC), a feedforward (FF) control method specifically tailored to suppress these coupled vibrations. Theoretically, DD-VSC suppresses coupled vibrations, and by introducing an additional degree-of-freedom in the FF controller structure, it mitigates discontinuities in FF controller outputs during fast and precise positioning. Its effectiveness was validated through experimental comparisons with the estimated response iterative tuning method using a laboratory-positioning device.

**Index Terms**—data-driven control, vibration suppression, coupled vibration, feedforward control, estimated response iterative tuning (ERIT)

## I. INTRODUCTION

Industrial mechatronic machines, such as logistics machinery and various machining tools, consist of numerous structural components. When the positioning mechanisms in these machines operate at high acceleration, coupled vibrations involving multiple structures arise [1], [2], [3]. For example, a stacker crane in automated storage and retrieval systems, which handles storage, conveyance, and retrieval of items in logistics facilities, is a tall positioning mechanism comprising a bottom frame, mast, lifting carriage with a fork, and top frame. Both the bottom and top frames must be precisely positioned to accurately and safely load and unload items. However, coupled vibrations occur during high-acceleration positioning owing to the flexibility of the mast [1], [4]. These vibrations degrade the task efficiency and precision of equipment, leading to the development of various vibration suppression control (VSC) methods, e.g., [5], [6]. Model-based feedforward (FF) control is particular

popular for vibration suppression, as it provides a broader control bandwidth than feedback (FB) control [7], [8]. However, achieving optimal control performance requires precise system identification and complex parameter tuning, which require significant design effort from engineers.

Recently, data-driven FF control approaches have attracted attention. For example, estimated response iterative tuning (ERIT) [9], [10] designs an FF controller using a single positioning experiment, offering a more efficient alternative to iterative learning control [11], which designs an FF controller by repeatedly performing positioning operations. ERIT predicts the responses of a plant using learning data from a single preliminary positioning experiment, and the FF controller, which outputs the FF control input, is then obtained by solving an optimization problem based on these predicted responses. However, before designing the data-driven controller, a reference model must be determined as an FF controller, which generates a trajectory reference to the FB control system. Selecting an appropriate reference for suppressing coupled vibrations can be challenging when the plant characteristics are unknown [12], often resulting in considerable effort to tune the desired response characteristics. The data-driven FF method presented in [13], which corresponds to the case where the reference model in ERIT is set to 1, also cannot be considered a suitable approach for suppressing coupled vibrations. Furthermore, no studies have yet applied ERIT to coupled vibration systems.

The joint input shaping and feedforward (JIS-FF) in [14] is a state-of-the-art data-driven FF control method known for its effectiveness in suppressing vibrations. This method is based on vibration suppression principles using model matching, where multiple FF controllers are designed through a predicted response-based optimization problem. However, the response characteristics of coupled vibration systems have not been fully analyzed in the literature. Furthermore, applying the method in [14] directly to fast, precise positioning tasks often

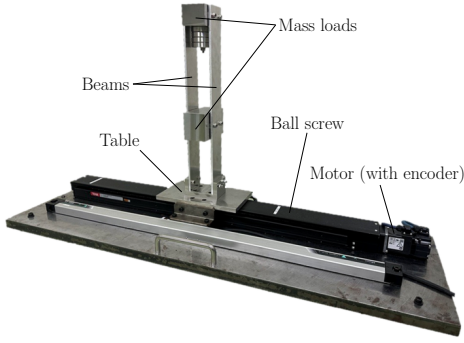


Fig. 1. The laboratory positioning device used for experiments.

results in discontinuities in the FF controller outputs.

This paper presents a data-driven vibration-suppression FF control (DD-VSC) method tailored for fast and precise positioning in coupled vibration systems. While the basic design theory of DD-VSC is similar to that of the JIS-FF method, this study extends the method by introducing a smoothing filter to basis functions of FF controllers to address output discontinuities in the FF control. Furthermore, the response characteristics of DD-VSC in coupled vibration systems are theoretically analyzed. Experimental results obtained within a laboratory positioning device emulating a stacker crane validate the effectiveness of DD-VSC compared to the ERIT method.

## II. PROBLEM STATEMENT

### A. Controlled Object

The experimental positioning device used as the controlled object is shown in Fig. 1. This device was designed to emulate a stacker crane commonly found in logistics facilities. Two mass loads are mounted on the moving table through two beams, emulating the resonance vibrations of a stacker crane [1], [4], [5], [6]. The table is driven by a servo motor and a ball screw. The angular position of the motor, detected by an encoder, is fed back to control the positions of both the table and the upper mass load. Control calculations are performed using a prototyping system (MicroLabBox, dSPACE) with a control period of  $T_s = 500 \mu s$ . In this study, the angular position of the motor is represented as the table position  $y_T$  (in the translational system), considering the ball screw pitch (20 mm/rev). The upper load position,  $y_L$ , is measured using a laser displacement sensor (LK-G505, Keyence) for system identification and to evaluate positioning performance.

The plant frequency responses from the motor torque reference  $u$  to  $y_T$  and  $y_L$ , measured using the sinusoidal sweep method, are depicted in Fig. 2. The positioning mechanism exhibits two prominent resonance modes at approximately 29 Hz and 72 Hz, owing to the mass loads, demonstrating typical coupled vibration characteristics with load resonance. Although not clearly visible in the figure, gain reduction and phase lead due to friction [15] occur in the low-frequency region. The discrete-time transfer functions for the plant, neglecting frictional nonlinearities and the differences in

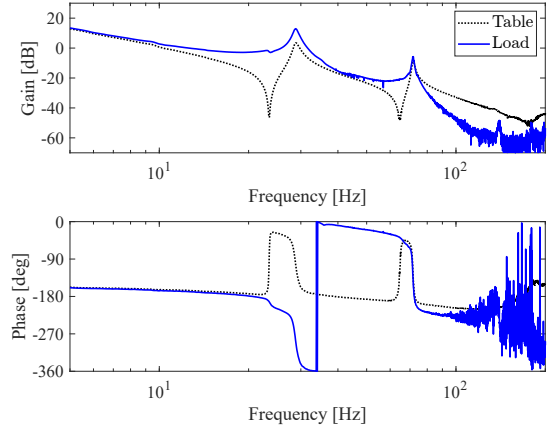


Fig. 2. Frequency characteristics of the plant.

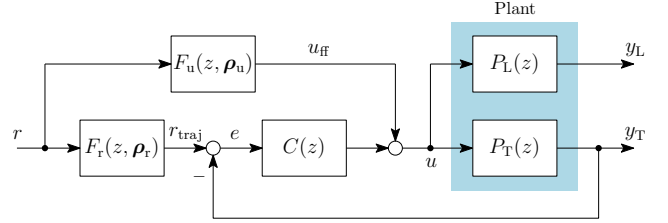


Fig. 3. Block diagram of the 2DoF positioning control system.

sensor characteristics between the table and the load, are expressed as (1).

$$P_T(z) = \frac{N_T(z)}{D(z)}, \quad P_L(z) = \frac{N_L(z)}{D(z)} \quad (1)$$

where  $P_T(z)$  and  $P_L(z)$  denote the transfer functions for the table and the upper load, respectively;  $N_T(z)$  and  $N_L(z)$  represent their corresponding numerator polynomials; and  $D(z)$  is the common denominator polynomial for both  $P_T(z)$  and  $P_L(z)$  owing to the coupled vibration system. The polynomials  $N_T(z)$ ,  $N_L(z)$ , and  $D(z)$  are derived through coprime factorization of  $P_T(z)$  and  $P_L(z)$ .

The target control specification for the plant is to achieve point-to-point positioning over a stroke of  $Y_r = 20$  mm, ensuring that both the table and load positions settle within  $\pm 50 \mu m$  of the target position within 0.15 s. To achieve fast and precise positioning performance, the control system must be designed to effectively suppress coupled vibrations between the table and mass loads.

### B. Control Problem

The block diagram of the two-degree-of-freedom (2DoF) positioning control system considered in this study is shown in Fig. 3. Here,  $r$  is the position command,  $r_{traj}$  is the table position trajectory reference,  $u_{ff}$  is the FF control input, and  $e$  is the table position tracking error. The feedback (FB) controller is represented by  $C(z)$ , whereas  $F_r(z, \rho_r)$  and  $F_u(z, \rho_u)$  represent FF controllers, with parameter vectors  $\rho_r$  and  $\rho_u$  to be designed. The control objective is to design FF controllers  $F_r(z, \rho_r)$  and  $F_u(z, \rho_u)$  that meet the target

control specification, assuming the true plant dynamics  $P_T(z)$  and  $P_L(z)$  are unknown. These FF controllers are designed in a data-driven manner, using learning data from a single preliminary positioning experiment (excluding  $y_L$ ).

For theoretical development, we define a discrete-time, linear time-invariant system  $S$  with input  $x(t)$  and output  $y(t)$ , represented in the lifted system form as follows:

$$\mathbf{y} = \mathbf{S}\mathbf{x} \quad (2)$$

with

$$\begin{aligned} \mathbf{y} &= \begin{bmatrix} y(0) & y(1) & \cdots & y(N-1) \end{bmatrix}^\top \in \mathbb{R}^N \\ \mathbf{x} &= \begin{bmatrix} x(0) & x(1) & \cdots & x(N-1) \end{bmatrix}^\top \in \mathbb{R}^N \end{aligned} \quad (3)$$

where  $\mathbf{S} \in \mathbb{R}^{N \times N}$  denotes the lower triangular impulse response matrix of  $S$  [16].

### III. DATA-DRIVEN FF CONTROL

This section provides a specific theoretical formulation of the data-driven optimization problems in both the ERIT and DD-VSC methods and analyzes their response characteristics in a coupled vibration system.

#### A. Conventional Method: ERIT

1) *Controller Structure*: In ERIT [9], [10], [12], the FF controller  $F_r(z, \rho_r)$ , which generates the position trajectory reference  $r_{\text{traj}}$ , is predetermined by a reference model  $T_{\text{ref}}(z)$  specifying an ideal response characteristic from  $r$  to  $y_T$ . Subsequently, another FF controller,  $F_u(z, \rho_u)$ , is designed in a data-driven manner to generate the FF control input  $u_{\text{ff}}$ . The FF controllers are defined as follows:

$$\begin{aligned} F_r(z) &= T_{\text{ref}}(z) \\ F_u(z, \rho_u) &= \Psi(z)\rho_u^\top \end{aligned} \quad (4)$$

with

$$\begin{aligned} \Psi(z) &= \begin{bmatrix} \Psi_0(z) & \Psi_1(z) & \cdots & \Psi_M(z) \end{bmatrix} \in \mathbb{C}^{1 \times (M+1)} \\ \rho_u &= \begin{bmatrix} \rho_{u0} & \rho_{u1} & \cdots & \rho_{uM} \end{bmatrix} \in \mathbb{R}^{1 \times (M+1)} \end{aligned} \quad (5)$$

where  $\Psi_m(z)$ ,  $m = 0, 1, \dots, M$  denote the basis functions, and  $\rho_{um}$ ,  $m = 0, 1, \dots, M$  denote the corresponding parameters. In this study,  $F_u(z, \rho_u)$  was set to have a linear parameter structure with respect to  $\rho_u$  for simplicity.

2) *Optimization Problem*: The undetermined parameter vector  $\rho_u$  in  $F_u(z, \rho_u)$  is designed by solving the following optimization problem, which aims to minimize the predicted tracking error  $\hat{e}(t, \rho_u) = r_{\text{traj}}(t) - \hat{y}_T(t, \rho_u)$  over the time interval  $t \in [0, T_{\text{ed}} - 1]$ .

$$\min_{\rho_u} \mathcal{J}(\rho_u) \quad (6)$$

with

$$\begin{aligned} \mathcal{J}(\rho_u) &= \|\hat{e}(\rho_u)\|_2 \\ \hat{e}(\rho_u) &= \begin{bmatrix} \hat{e}(0, \rho_u) & \hat{e}(1, \rho_u) & \cdots & \hat{e}(T_{\text{ed}} - 1, \rho_u) \end{bmatrix}^\top \in \mathbb{R}^{T_{\text{ed}}} \end{aligned} \quad (7)$$

where  $T_{\text{ed}}$  denotes the prediction termination time. Note that, since  $F_r(z) = T_{\text{ref}}(z)$ , as stated in (4), the trajectory reference  $r_{\text{traj}}$  is fixed.

The actual table position tracking error  $e(t, \rho_u)$ , as shown in Fig. 3 at  $t \in [0, T_{\text{ed}} - 1]$ , is expressed as

$$\begin{aligned} e(\rho_u) &= \begin{bmatrix} e(0, \rho_u) & e(1, \rho_u) & \cdots & e(T_{\text{ed}} - 1, \rho_u) \end{bmatrix}^\top \\ &= \mathbf{r}_{\text{traj}} - (\mathbf{I} + \mathbf{P}_T \mathbf{C})^{-1} \mathbf{P}_T (\mathbf{C} \mathbf{r}_{\text{traj}} + \mathbf{F}_u(\rho_u) \mathbf{r}) \end{aligned} \quad (8)$$

with

$$\begin{aligned} \mathbf{r} &= \begin{bmatrix} r(0) & r(1) & \cdots & r(T_{\text{ed}} - 1) \end{bmatrix}^\top \in \mathbb{R}^{T_{\text{ed}}} \\ \mathbf{r}_{\text{traj}} &= \begin{bmatrix} r_{\text{traj}}(0) & r_{\text{traj}}(1) & \cdots & r_{\text{traj}}(T_{\text{ed}} - 1) \end{bmatrix}^\top \in \mathbb{R}^{T_{\text{ed}}} \end{aligned} \quad (9)$$

where  $\mathbf{P}_T \in \mathbb{R}^{T_{\text{ed}} \times T_{\text{ed}}}$ ,  $\mathbf{C} \in \mathbb{R}^{T_{\text{ed}} \times T_{\text{ed}}}$ , and  $\mathbf{F}_u(\rho_u) \in \mathbb{R}^{T_{\text{ed}} \times T_{\text{ed}}}$  are the matrices corresponding to  $P_T(z)$ ,  $C(z)$ , and  $F_u(z, \rho_u)$ , respectively. In a data-driven design problem, since an accurate mathematical model of  $P_T(z)$  is absent,  $\hat{e}(t, \rho_u)$  cannot be calculated directly from (8). Therefore,  $\hat{e}(t, \rho_u)$  is predicted using the learning data acquired by a single preliminary positioning experiment. In this study, the predicted  $\hat{e}(\rho_u)$  in (7) is calculated as follows based on the method in [16], [17]:

$$\begin{aligned} \hat{e}(\rho_u) &= \mathbf{r}_{\text{traj}} - \hat{\mathbf{G}} (\mathbf{C} \mathbf{r}_{\text{traj}} + \mathbf{F}_u(\rho_u) \mathbf{r}) \\ &= \Phi_r - \Phi_u \rho_u^\top \end{aligned} \quad (10)$$

with

$$\begin{aligned} \hat{\mathbf{G}} &= \mathbf{Y}_T^{\text{lrn}} (\mathbf{C} \mathbf{R}_{\text{traj}}^{\text{lrn}} + \mathbf{U}_{\text{ff}}^{\text{lrn}})^{-1} \in \mathbb{R}^{T_{\text{ed}} \times T_{\text{ed}}} \\ \Phi_r &= (\mathbf{I} - \hat{\mathbf{G}} \mathbf{C}) \mathbf{r}_{\text{traj}} \in \mathbb{R}^{T_{\text{ed}}} \\ \Phi_u &= \hat{\mathbf{G}} \begin{bmatrix} \Psi_0 \mathbf{r} & \Psi_1 \mathbf{r} & \cdots & \Psi_M \mathbf{r} \end{bmatrix} \in \mathbb{R}^{T_{\text{ed}} \times (M+1)} \end{aligned} \quad (11)$$

where  $\mathbf{Y}_T^{\text{lrn}} \in \mathbb{R}^{T_{\text{ed}} \times T_{\text{ed}}}$ ,  $\mathbf{R}_{\text{traj}}^{\text{lrn}} \in \mathbb{R}^{T_{\text{ed}} \times T_{\text{ed}}}$ , and  $\mathbf{U}_{\text{ff}}^{\text{lrn}} \in \mathbb{R}^{T_{\text{ed}} \times T_{\text{ed}}}$  represent the Toeplitz matrices using the learning data  $y_T^{\text{lrn}}(t)$ ,  $r_{\text{traj}}^{\text{lrn}}(t)$ , and  $u_{\text{ff}}^{\text{lrn}}(t)$  at  $t = 0, 1, \dots, T_{\text{ed}} - 1$ , respectively, while  $\Psi_m$ ,  $m = 0, 1, \dots, M$  are the matrices corresponding to  $\Psi_m(z)$  in (5). Therefore, by defining the objective function  $\mathcal{J}(\rho_u)$  using (10) and (11), and solving the optimization problem in (6), the optimal parameter vector  $\rho_u^*$  can be obtained in a data-driven manner. When  $F_u(z, \rho_u)$  is linear in  $\rho_u$  and  $\Phi_u^\top \Phi_u \succ 0$ ,  $\rho_u^*$  is obtained from (12) as an analytical solution, using the least-squares method.

$$\rho_u^{*\top} = (\Phi_u^\top \Phi_u)^{-1} \Phi_u^\top \Phi_r \quad (12)$$

3) *Response Characteristics*: The response characteristics are considered when the designed FF controllers are applied to a coupled vibration system. If  $\rho_u^*$  that ideally satisfies  $e(t) = 0$  in Fig. 3 is obtained, then  $F_u(z, \rho_u^*)$  is formulated as [8], [9], [10], [14]

$$F_u(z, \rho_u^*) = \frac{T_{\text{ref}}(z)}{P_T(z)} = \frac{D(z)}{N_T(z)} T_{\text{ref}}(z) \quad (13)$$

In this case, the transfer characteristics of the table and load positions can be formulated as follows:

$$\begin{aligned} y_T(z, \boldsymbol{\rho}_u^*) &= T_{\text{ref}}(z)r(z) = r_{\text{traj}}(z) \\ y_L(z, \boldsymbol{\rho}_u^*) &= \frac{N_L(z)}{N_T(z)} T_{\text{ref}}(z)r(z) \end{aligned} \quad (14)$$

Equation (14) implies that although the table position  $y_T$  perfectly follows the trajectory reference  $r_{\text{traj}}$  specified by  $T_{\text{ref}}(z)$ , the load position  $y_L$  results in vibratory responses owing to the poles in  $N_T(z)$ . To suppress these vibratory responses,  $T_{\text{ref}}(z)$  must possess characteristics that cancel out the undesirable poles. However, in a data-driven design approach that does not rely on accurate models or precise knowledge of the plant, determining an appropriate  $T_{\text{ref}}(z)$  is practically challenging. Therefore, ERIT cannot be considered a suitable method for suppressing coupled vibrations.

### B. Proposed Method: DD-VSC

Considering the issues with ERIT described in Sect. III-A, a DD-VSC is proposed to ensure vibration suppression in coupled vibration systems. The basic controller design theory of DD-VSC is based on JIS-FF [14] and is extended to a more practical design framework that includes measures for mitigating discontinuities in the FF outputs.

1) *Controller Structure:* In DD-VSC, both FF controllers,  $F_r(z, \boldsymbol{\rho}_r)$  and  $F_u(z, \boldsymbol{\rho}_u)$ , are defined using the undetermined parameter vectors,  $\boldsymbol{\rho}_r$  and  $\boldsymbol{\rho}_u$ , as follows:

$$\begin{aligned} F_r(z, \boldsymbol{\rho}_r) &= \boldsymbol{\Psi}^\dagger(z) \boldsymbol{\rho}_r^\top \\ F_u(z, \boldsymbol{\rho}_u) &= \boldsymbol{\Psi}^\dagger(z) \boldsymbol{\rho}_u^\top \end{aligned} \quad (15)$$

with

$$\begin{aligned} \boldsymbol{\Psi}_m^\dagger(z) &= Q(z)z^{-m} \\ \boldsymbol{\Psi}^\dagger(z) &= \begin{bmatrix} \boldsymbol{\Psi}_0^\dagger(z) & \boldsymbol{\Psi}_1^\dagger(z) & \cdots & \boldsymbol{\Psi}_M^\dagger(z) \end{bmatrix} \in \mathbb{C}^{1 \times (M+1)} \\ \boldsymbol{\rho}_r &= \begin{bmatrix} \rho_{r0} & \rho_{r1} & \cdots & \rho_{rM} \end{bmatrix} \in \mathbb{R}^{1 \times (M+1)} \\ \boldsymbol{\rho}_u &= \begin{bmatrix} \rho_{u0} & \rho_{u1} & \cdots & \rho_{uM} \end{bmatrix} \in \mathbb{R}^{1 \times (M+1)} \end{aligned} \quad (16)$$

where  $\boldsymbol{\Psi}_m^\dagger(z)$ ,  $m = 0, 1, \dots, M$  denote the basis functions, including an arbitrary, stable low-pass filter  $Q(z)$ . Introducing  $Q(z)$  into the basis functions to smooth the FF outputs represents an extension of DD-VSC compared to JIS-FF in [14].

2) *Optimization Problem:* The parameter vectors,  $\boldsymbol{\rho}_r$  and  $\boldsymbol{\rho}_u$ , are designed using the following optimization problem to minimize the predicted tracking error  $\hat{e}(t, \boldsymbol{\rho}_r, \boldsymbol{\rho}_u) = r_{\text{traj}}(t, \boldsymbol{\rho}_r) - \hat{y}_T(t, \boldsymbol{\rho}_r, \boldsymbol{\rho}_u)$  at  $t \in [0, T_{\text{ed}} - 1]$ .

$$\begin{aligned} \min_{\boldsymbol{\rho}_r, \boldsymbol{\rho}_u} \quad & \mathcal{J}^\dagger(\boldsymbol{\rho}_r, \boldsymbol{\rho}_u) \\ \text{s.t.} \quad & \mathcal{C}(\boldsymbol{\rho}_r) \end{aligned} \quad (17)$$

with

$$\begin{aligned} \mathcal{J}^\dagger(\boldsymbol{\rho}_r, \boldsymbol{\rho}_u) &= \|\hat{e}(\boldsymbol{\rho}_r, \boldsymbol{\rho}_u)\|_2 \\ \hat{e}(\boldsymbol{\rho}_r, \boldsymbol{\rho}_u) &= \begin{bmatrix} \hat{e}(0, \boldsymbol{\rho}_r, \boldsymbol{\rho}_u) & \hat{e}(1, \boldsymbol{\rho}_r, \boldsymbol{\rho}_u) \\ \cdots & \hat{e}(T_{\text{ed}} - 1, \boldsymbol{\rho}_r, \boldsymbol{\rho}_u) \end{bmatrix}^\top \in \mathbb{R}^{T_{\text{ed}}} \end{aligned} \quad (18)$$

The objective function  $\mathcal{J}^\dagger(\boldsymbol{\rho}_r, \boldsymbol{\rho}_u)$  in (18) is similar to that of ERIT in (7); however, the position trajectory reference  $r_{\text{traj}}$  varies with respect to  $\boldsymbol{\rho}_r$ . Furthermore, an equality constraint  $\mathcal{C}(\boldsymbol{\rho}_r)$  is introduced to ensure that  $r_{\text{traj}}$  settles to the target position, as shown in (17).

According to the Youla parameterization [18], FF controllers that can place any pole in the transfer characteristic from  $r$  to  $y_T$  are expressed as follows:

$$\begin{aligned} F_r(z, \boldsymbol{\rho}_r) &= N_T(z)H(z) \\ F_u(z, \boldsymbol{\rho}_u) &= D(z)H(z) \end{aligned} \quad (19)$$

Here,  $H(z)$  is an arbitrary, stable transfer function. When the FF controllers shown in (19) are applied to the 2DoF control system in Fig. 3,  $e = 0$  holds. Hence, the predicted tracking error is used as the objective function to realize (19). By introducing an undetermined parameter vector  $\boldsymbol{\rho} = [\boldsymbol{\rho}_r \ \boldsymbol{\rho}_u] \in \mathbb{R}^{1 \times 2(M+1)}$ ,  $\hat{e}(\boldsymbol{\rho}_r, \boldsymbol{\rho}_u)$  in (18) is formulated as follows, using  $\hat{\mathbf{G}}$  in (11):

$$\begin{aligned} \hat{e}(\boldsymbol{\rho}) &= F_r(\boldsymbol{\rho}_r)r - \hat{\mathbf{G}}(CF_r(\boldsymbol{\rho}_r) + F_u(\boldsymbol{\rho}_u))r \\ &= \left[ (\mathbf{I} - \hat{\mathbf{G}}C)\boldsymbol{\Psi}_r^\dagger \quad -\hat{\mathbf{G}}\boldsymbol{\Psi}_r^\dagger \right] \boldsymbol{\rho}^\top = \boldsymbol{\Phi}^\dagger \boldsymbol{\rho}^\top \end{aligned} \quad (20)$$

with

$$\boldsymbol{\Psi}_r^\dagger = \begin{bmatrix} \boldsymbol{\Psi}_0^\dagger r & \boldsymbol{\Psi}_1^\dagger r & \cdots & \boldsymbol{\Psi}_M^\dagger r \end{bmatrix} \in \mathbb{R}^{T_{\text{ed}} \times (M+1)} \quad (21)$$

where  $\boldsymbol{\Psi}_m^\dagger \in \mathbb{R}^{T_{\text{ed}} \times T_{\text{ed}}}$ ,  $m = 0, 1, \dots, M$  are the matrices corresponding to  $\boldsymbol{\Psi}_m^\dagger(z)$  in (16). Therefore, the objective function  $\mathcal{J}^\dagger(\boldsymbol{\rho}_r, \boldsymbol{\rho}_u)$  in (18) can be defined as

$$\mathcal{J}^\dagger(\boldsymbol{\rho}) = \boldsymbol{\rho} \boldsymbol{\Phi}^{\dagger\top} \boldsymbol{\Phi}^\dagger \boldsymbol{\rho}^\top \quad (22)$$

Subsequently, the equality constraint,  $\mathcal{C}(\boldsymbol{\rho}_r)$  in (17), for ensuring  $r_{\text{traj}} = r$  in the steady state is formulated as follows, considering  $F_r(1, \boldsymbol{\rho}_r) = 1$ :

$$\mathcal{C}(\boldsymbol{\rho}) : \begin{bmatrix} \boldsymbol{\Psi}^\dagger(1) & \mathbf{O}_{1 \times (M+1)} \end{bmatrix} \boldsymbol{\rho}^\top = \boldsymbol{\Sigma}_r \boldsymbol{\rho}^\top = 1 \quad (23)$$

Therefore, using (22) and (23), when  $F_r(z, \boldsymbol{\rho}_r)$  and  $F_u(z, \boldsymbol{\rho}_u)$  are linear in  $\boldsymbol{\rho}_r$  and  $\boldsymbol{\rho}_u$ , respectively, and  $\boldsymbol{\Phi}^{\dagger\top} \boldsymbol{\Phi}^\dagger \succ 0$  and  $\boldsymbol{\Sigma}_r (\boldsymbol{\Phi}^{\dagger\top} \boldsymbol{\Phi}^\dagger)^{-1} \boldsymbol{\Sigma}_r^\top \neq 0$ , the optimal parameter vector  $\boldsymbol{\rho}^* = [\boldsymbol{\rho}_r^* \ \boldsymbol{\rho}_u^*]$  of (17) can be analytically obtained from (24) using the Lagrange multiplier method.

$$\boldsymbol{\rho}^{*\top} = \left\{ \boldsymbol{\Sigma}_r (\boldsymbol{\Phi}^{\dagger\top} \boldsymbol{\Phi}^\dagger)^{-1} \boldsymbol{\Sigma}_r^\top \right\}^{-1} (\boldsymbol{\Phi}^{\dagger\top} \boldsymbol{\Phi}^\dagger)^{-1} \boldsymbol{\Sigma}_r^\top \quad (24)$$

3) *Response Characteristics:* As with ERIT, the response characteristics of DD-VSC in a coupled vibration system are analyzed. In the case where the order  $M$  of the FF controllers exceeds that of the plant, the transfer characteristics of the table and load positions are formulated as follows, when  $\boldsymbol{\rho}_r^*$  and  $\boldsymbol{\rho}_u^*$  achieve  $e = 0$  [8]:

$$\begin{aligned} y_T(z, \boldsymbol{\rho}_r^*, \boldsymbol{\rho}_u^*) &= N_T(z)Q(z)F_{\text{red}}(z, \boldsymbol{\rho}_r^*, \boldsymbol{\rho}_u^*)r(z) \\ y_L(z, \boldsymbol{\rho}_r^*, \boldsymbol{\rho}_u^*) &= N_L(z)Q(z)F_{\text{red}}(z, \boldsymbol{\rho}_r^*, \boldsymbol{\rho}_u^*)r(z) \end{aligned} \quad (25)$$

where  $F_{\text{red}}(z, \boldsymbol{\rho}_r^*, \boldsymbol{\rho}_u^*)$  is the redundant polynomial when the order  $M$  is higher than that of the plant. From (25), both the table and load responses share common poles, arbitrarily

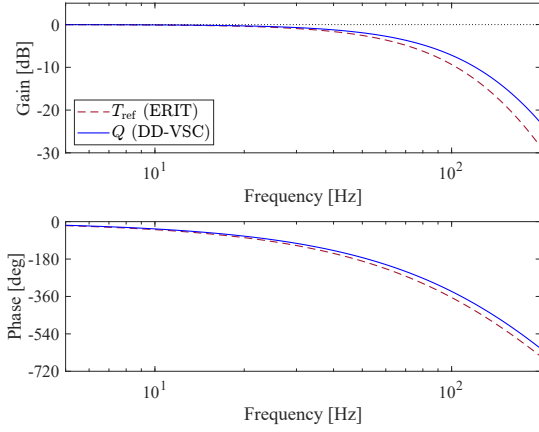


Fig. 4. Frequency characteristics of the reference model  $T_{\text{ref}}(z)$  and the smoothing filter  $Q(z)$ .

defined by  $Q(z)$ , indicating that DD-VSC can suppress coupled vibrations. Additionally, the FF outputs,  $r_{\text{traj}}$  and  $u_{\text{ff}}$ , can be smoothed owing to the low-pass characteristic of  $Q(z)$  included in the basis functions in (16). Furthermore, assuming  $e = \hat{e} = 0$ , the following relationship is satisfied:

$$\frac{F_r(z, \rho_r^*)}{F_u(z, \rho_u^*)} = \frac{N_T(z)}{D(z)} = P_T(z) \quad (26)$$

Equation (26) implies that DD-VSC achieves model matching with the plant through the optimization problem in (17) [14]. Thus, DD-VSC theoretically enables vibration suppression in coupled vibration systems, offering a potential solution to the issues presented in the ERIT.

#### IV. EXPERIMENTAL EVALUATION

##### A. Experimental Conditions

Positioning experiments were performed using the 2DoF control system shown in Fig. 3. The FB controller  $C(z)$  employed a PID compensator, with parameters tuned to achieve an open-loop gain crossover frequency of approximately 20 Hz. A third-order S-shaped position command, with a stroke of 20 mm, a settling time of 0.125 s, and a maximum acceleration of  $\pm 0.5$  G, was used as the position command  $r$ .

The settings for each data-driven FF method are described below. In the ERIT approach, the reference model  $T_{\text{ref}}(z)$  was predefined as the following tenth-order low-pass filter, designed without specific knowledge of the resonance modes present in the plant.

$$T_{\text{ref}}(z) = \left\{ \frac{(1 - e^{-\omega_{\text{ref}} T_s}) z}{z - e^{-\omega_{\text{ref}} T_s}} \right\}^{10} \quad (27)$$

where  $\omega_{\text{ref}}$  denotes the cutoff frequency, set to  $\omega_{\text{ref}} = 2\pi \cdot 200$  rad/s, allowing  $r_{\text{traj}}$  to approach the target position within the specific settling time. The frequency characteristics of

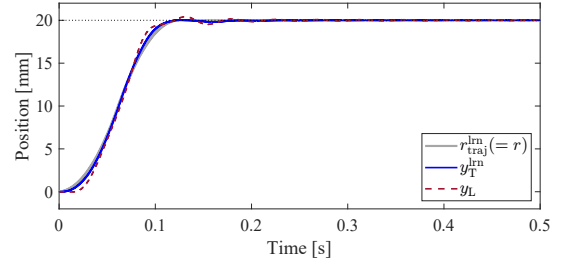


Fig. 5. Response waveforms of the positioning experiment for acquisition of learning data.

$T_{\text{ref}}(z)$  are shown in Fig. 4. The FF controller  $F_u(z)$  is defined as (28) with  $M = 10$ .

$$F_u(z, \rho_u) = \Psi(z) \rho_u \quad (28)$$

$$\Psi(z) = T_{\text{ref}}(z) \begin{bmatrix} 1 & z^{-1} & \dots & z^{-10} \end{bmatrix} \in \mathbb{C}^{1 \times 11}$$

In the DD-VSC approach, the order of the FF controllers was set to  $M = 10$ , and the smoothing filter  $Q(z)$  was implemented as the following low-pass filter.

$$Q(z) = \left\{ \frac{(1 - e^{-\omega_Q T_s}) z}{z - e^{-\omega_Q T_s}} \right\}^{10} \quad (29)$$

The cutoff frequency  $\omega_Q$  in (29) was set to  $\omega_Q = 2\pi \cdot 230$  rad/s, enabling  $r_{\text{traj}}$  to reach the target position by the desired settling time while smoothing both  $r_{\text{traj}}$  and  $u_{\text{ff}}$ . Specifically, in this study, since the amplitude of  $u_{\text{ff}}$  tends to become large,  $\omega_Q$  was adjusted to ensure that the control input remains within the limits of the experimental system. The frequency characteristics of  $Q(z)$  are presented in Fig. 4. Note that in both methods, the orders of the basis functions and filters, as well as each cutoff frequency, were determined through a trial-and-error process. However, they can be easily adjusted by verifying the predicted responses without the need for conducting experiments.

As a common configuration for both methods, learning data—comprising  $y_T^{\text{lrn}}$ ,  $r_{\text{traj}}^{\text{lrn}}$ , and  $u_{\text{ff}}^{\text{lrn}}$ —were collected through a single positioning experiment using a one-degree-of-freedom control system, with  $F_r(z) = 1$  and  $F_u(z) = 0$  in Fig. 3. The response waveforms of the learning data  $r_{\text{traj}}^{\text{lrn}} (= r)$  and  $y_T^{\text{lrn}}$  (with the load position  $y_L$  shown for reference) are shown in Fig. 5. The prediction termination time,  $T_{\text{ed}}$ , was set to 1000 (i.e.,  $T_{\text{ed}} T_s = 0.5$  s) to evaluate the interval needed for the table position to settle sufficiently to the target position.

##### B. Designed FF Controllers

The frequency characteristics of the FF controllers,  $F_r(z)$  and  $F_u(z)$ , designed using the ERIT and DD-VSC methods, are shown in Fig. 6 and Fig. 7, respectively. In DD-VSC,  $F_r(z)$  reduces gain near the first antiresonance frequency, approximately 23 Hz, as shown in Fig. 6, whereas  $F_u(z)$  slightly reduces gain near the first resonance frequency, approximately 29 Hz in Fig. 7. This implies that, despite the impact of neglected friction and plant uncertainties on response prediction accuracy, DD-VSC designs FF controllers

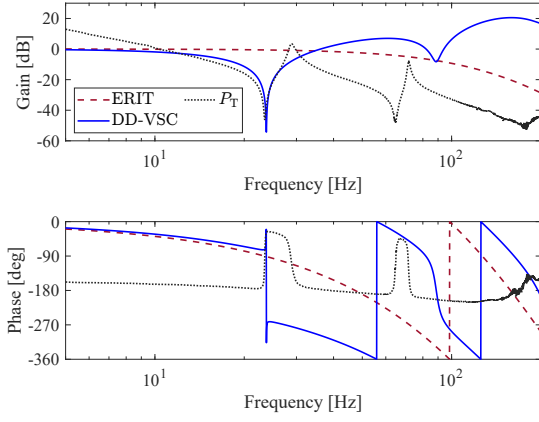


Fig. 6. Frequency characteristics of  $F_r(z)$  designed using ERIT and DD-VSC.

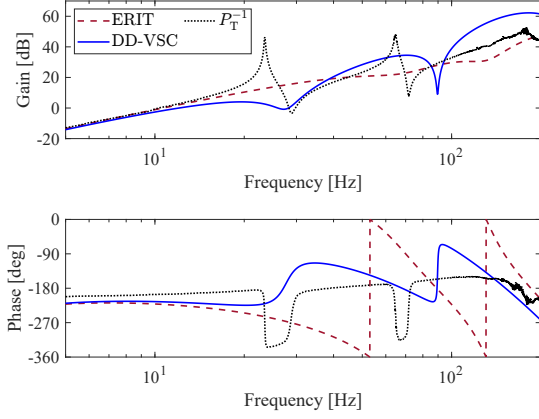


Fig. 7. Frequency characteristics of  $F_u(z)$  designed using ERIT and DD-VSC.

for achieving the response characteristics outlined in (25). In contrast, with ERIT, since  $F_r(z)$  is fixed to  $T_{\text{ref}}(z)$  without addressing vibration suppression,  $F_u(z)$  exhibits a different frequency shaping compared to DD-VSC.

Subsequently, the table position trajectory reference  $r_{\text{traj}}$  and the FF control input  $u_{\text{ff}}$ , generated by the designed FF controllers, are shown in Fig. 8. DD-VSC generates oscillatory  $u_{\text{ff}}$  at the acceleration sign-switching timings in the position command  $r$  to actively suppress coupled vibrations. Although the input amplitude of  $u_{\text{ff}}$  is larger than that in ERIT, the smoothing filter  $Q(z)$  effectively mitigates discontinuities in both  $r_{\text{traj}}$  and  $u_{\text{ff}}$ , ensuring that  $u_{\text{ff}}$  satisfies the input limit of  $u$  set to  $\pm 8$  V in the experimental system. As an additional comparison, the FF control input waveform designed using the JIS-FF method in [14] (with the FF controller order of 10) is shown in Fig. 9. The JIS-FF method fails to generate feasible FF outputs suitable for fast and precise positioning.

### C. Experimental Results

The positioning experiment was conducted using a 2DoF control system, with FF controllers designed according to each method. The response waveforms for the table and load positions,  $y_T$  and  $y_L$ , along with their respective position

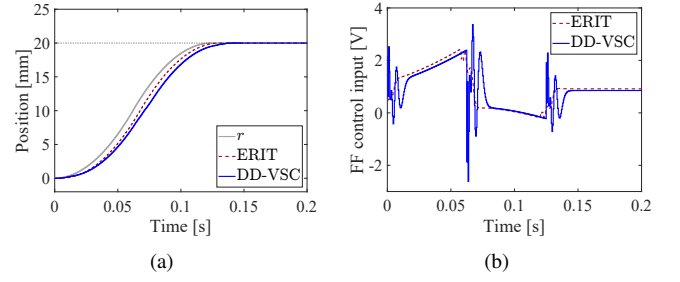


Fig. 8. Waveforms of FF controller outputs designed using ERIT and DD-VSC: (a) table position trajectory reference  $r_{\text{traj}}$ ; (b) FF control input  $u_{\text{ff}}$ .

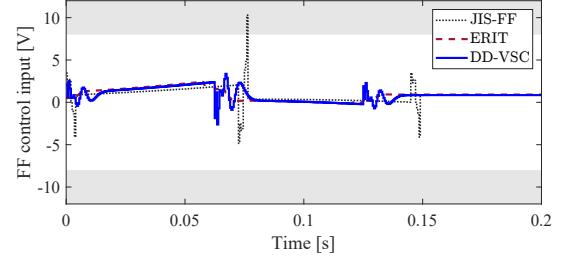


Fig. 9. Waveform of FF control input  $u_{\text{ff}}$  designed using JIS-FF.

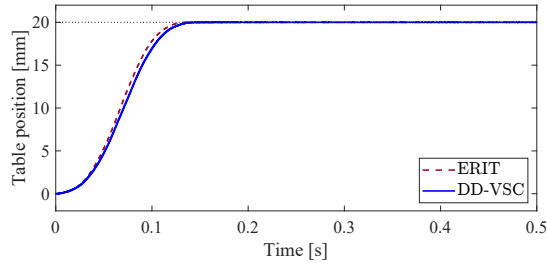
errors,  $Y_r - y_T$  and  $Y_r - y_L$ , are shown in Fig. 10 and Fig. 11. With ERIT, the table position satisfied the target control specification; however, the load position exhibited significant residual vibrations near the target position, exceeding the target settling accuracy of  $\pm 50$   $\mu\text{m}$ . This vibration is primarily composed around the antiresonance frequency of the first resonance mode on the table side, corresponding to the effect of  $N_T(z)$  in (14) (actually, the FB control also impacts the vibratory response). In contrast, the DD-VSC method successfully suppressed residual vibrations in both positions, achieving a fine positioning that satisfies the target control specification.

To quantitatively evaluate the positioning performance, the root mean squared error (RMSE) and maximum absolute error (MAE) for  $Y_r - y_T$  and  $Y_r - y_L$  over the time interval  $[0.15, 0.50]$  s, as well as the settling times of  $y_T$  and  $y_L$ , are shown in Table I. The values shown in parentheses for DD-VSC represent the reduction rates relative to those by ERIT. DD-VSC outperforms ERIT across all aspects, demonstrating its effectiveness in suppressing coupled vibrations.

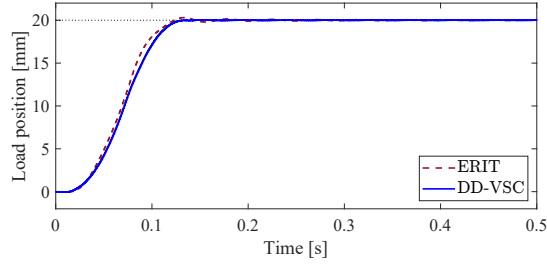
## V. CONCLUSION

This paper presents a data-driven, vibration-suppressing FF control method (DD-VSC) designed for fast and precise positioning control of coupled vibration systems. Building upon the JIS-FF method outlined in [14], DD-VSC extends its functionality by incorporating a smoothing filter  $Q(z)$  into the FF controller structure, effectively addressing issues such as FF output discontinuities. Furthermore, the response characteristics of the DD-VSC in coupled vibration systems were analyzed theoretically, highlighting its capability to



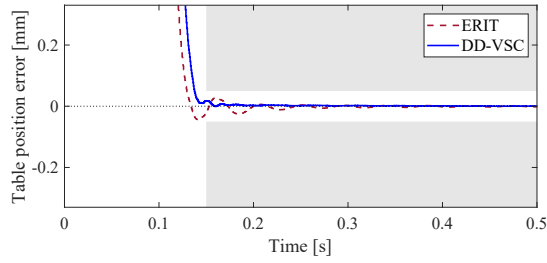


(a)

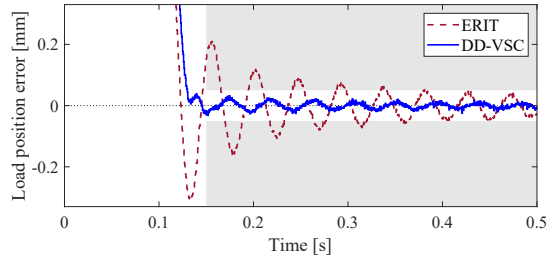


(b)

Fig. 10. Waveforms of the table and load positions achieved using ERIT and DD-VSC: (a) table position  $y_T$ ; (b) load position  $y_L$ .



(a)



(b)

Fig. 11. Waveforms of the table and load position errors achieved using ERIT and DD-VSC: (a) table position error  $Y_T - y_T$ ; (b) load position error  $Y_L - y_L$ .

effectively suppress coupled vibrations. Experimental results using a laboratory positioning device further validate the superior performance of DD-VSC, demonstrating a significant reduction in vibratory responses compared to ERIT, a conventional data-driven FF control method.

## REFERENCES

- [1] J. Ismail and S. Liu, "Control-oriented modeling and analysis of a flexible beam carrying a moving mass," in *Proc. Eur. Control Conf.*, 2020, pp. 1998–2003.

TABLE I  
QUANTITATIVE COMPARISON OF POSITIONING PERFORMANCE.

		ERIT	DD-VSC
RMSE [ $\mu\text{m}$ ]	Table	7.6	2.9 (61.8 %)
	Load	63.8	10.6 (83.4 %)
MAE [ $\mu\text{m}$ ]	Table	26.8	17.9 (33.2 %)
	Load	209.8	32.1 (84.7 %)
Settling time [s]	Table	0.15	0.15 (0.0 %)
	Load	0.38	0.15 (60.5 %)

- [2] T. Kai, H. Sekiguchi, and H. Ikeda, "Control structure with dual acceleration feedback for positioning machine with semi-closed servo system," *IEEE J. Ind. App.*, vol. 11, no. 2, pp. 351–358, 2022.
- [3] M. Iwasaki, K. Seki, and Y. Maeda, "High-precision motion control techniques: A promising approach to improving motion performance," *IEEE Ind. Electron. Mag.*, vol. 6, no. 1, pp. 32–40, 2012.
- [4] J. Diwold, B. Kolar, and M. Schöberl, "Flatness analysis for the sampled-data model of a single mast stacker crane," in *Proc. 12th IFAC Symp. Nonlinear Control Syst.*, 2023, pp. 222–227.
- [5] A. Galkina and K. Schlacher, "Flatness-based model predictive control with linear programming for a single mast stacker crane," in *Proc. 9th Vienna Int. Conf. Math. Modelling*, 2018, pp. 31–36.
- [6] G. Li, X. Ma, and Y. Li, "Robust command shaped vibration control for stacker crane subject to parameter uncertainties and external disturbances," *IEEE Trans. Ind. Electron.*, vol. 71, no. 11, pp. 14740–14752, 2024.
- [7] N.C. Singer and W.P. Seering, "Preshaping command inputs to reduce system vibration," *J. Dyn. Syst., Meas., Control*, vol. 112, no. 1, pp. 76–82, 1990.
- [8] Y. Maeda and M. Iwasaki, "Improvement of adaptive property by adaptive deadbeat feedforward compensation without convex optimization," *IEEE Trans. Ind. Electron.*, vol. 62, no. 1, pp. 466–474, 2015.
- [9] O. Kaneko and T. Nakamura, "Data-driven prediction of 2DOF control systems with updated feedforward controller," in *Proc. SICE Annu. Conf.*, 2017, pp. 259–262.
- [10] Y. Fujimoto, "Estimated response iterative tuning with signal projection," *IFAC J. Syst. Control*, vol. 19, 2022.
- [11] D.A. Bristow, M. Tharayil, and A.G. Alleyne, "A survey of iterative learning control," *IEEE Control Syst. Mag.*, vol. 26, no. 3, pp. 96–114, 2006.
- [12] S. Ishihara, "Designing reference model for estimated response iterative tuning by preference learning," in *Proc. IEEE 28th Int. Conf. Emerg. Technol. Factory Autom.*, 2023.
- [13] S.H. van der Meulen, R.L. Tousain, and O.H. Bosgra, "Fixed structure feedforward controller design exploiting iterative trials: Application to a wafer stage and a desktop printer," *J. Dyn. Syst. Meas. Control.*, vol. 130, no. 5, 051006, 2008.
- [14] F. Boeren, D. Bruijnen, N. van Dijk, and T. Oomen, "Joint input shaping and feedforward for point-to-point motion: Automated tuning for an industrial nanopositioning system," *Mechatron.*, vol. 24, no. 6, pp. 572–581, 2014.
- [15] Y. Maeda, K. Harata, and M. Iwasaki, "A friction model-based frequency response analysis for frictional servo systems," *IEEE Trans. Ind. Informat.*, vol. 14, no. 11, pp. 5246–5255, 2018.
- [16] Z. Zhang and W. Yin, "Data-driven feedforward control on active vibration isolation system," in *Proc. 17th Int. Conf. Control, Autom. and Syst.*, 2017, pp. 562–567.
- [17] D. Yamaguchi, S. Sato, and Y. Maeda, "Direct data-driven control-based additive feedforward compensation for fast and precise positioning control," in *Proc. 2024 IEEE/ASME Int. Conf. Adv. Intel. Mechatron.*, 2024, pp. 1203–1210.
- [18] D.C. Youla, H.A. Jabr, and J.J. Bongiorno, "Modern Wiener-Hopf design of optimal controllers—Part II: The multivariable case," *IEEE Trans. Autom. Control*, vol. 21, no. 3, pp. 319–338, 1976.